Tert-butyl peroxy radical: ground and first excited state energetics and fundamental frequencies

Journal:	*Physical Chemistry Chemical Physics*
Manuscript ID	CP-ART-03-2019-001476.R1
Article Type:	Paper
Date Submitted by the Author:	12-Apr-2019
Complete List of Authors:	Franke, Peter; University of Georgia, Department of Chemistry Moore, Kevin; University of Georgia, Computational Chemistry Schaefer, Henry; University of Georgia, Computational Chemistry Gary, Douberly; University of Georgia, Department of Chemistry

Tert-butyl peroxy radical: ground and first excited state energetics and fundamental frequencies†

Peter R. Franke[1], Kevin B. Moore III[1,2], Henry F. Schaefer III[1,2], and Gary E. Douberly[1,a]

[1] *Department of Chemistry, University of Georgia, Athens, GA, 30602*
[2] *Center for Computational Quantum Chemistry, University of Georgia, Athens, GA, 30602*
[a] *douberly@uga.edu*

† Electronic Supplementary Information (ESI) available: details of the treatment of anharmonic resonance polyads (matrix elements, Hamiltonian matrices, eigenvalues, and eigenvectors); Cartesian coordinates, harmonic frequencies, and harmonic intensities of all the optimized CCSD(T) geometries of the peroxy radical in the $\widetilde{\mathrm{X}}\ ^2A''$ and $\widetilde{\mathrm{A}}\ ^2A'$ electronic states, computed with the ANO0 and ANO1 basis sets and UHF and ROHF references; optimized coordinates along the peroxy torsional scan, at 5° increments.

1 Abstract

Alkylperoxy radicals ($RO_2^{\cdot}$) are key intermediates in combustion and atmospheric oxidation processes. As such, reliable detection and monitoring of these radicals can provide a wealth of information about the underlying chemistry. The *tert*-butyl peroxy radical is the archetypal tertiary peroxy radical, yet its vibrational spectroscopy is largely unexplored. To aid in future experimental investigations, we have performed high-level theoretical studies of the fundamental vibrational frequencies of the ground- and first excited states. A conformer search on both electronic surfaces reveals single minimum-energy structures. We predict an $\widetilde{\mathrm{A}}\ ^2A' \leftarrow \widetilde{\mathrm{X}}\ ^2A''$ adiabatic excitation energy of 7738 cm^{-1} via focal point analysis, approximating the CCSDT(Q)/CBS level of theory. This excitation energy agrees to within 17 cm^{-1} of the most accurate experimental measurement. We compute CCSD(T) fundamental vibrational frequencies via second-order vibrational perturbation theory (VPT2), using a hybrid force field in which the quadratic (cubic/quartic) force constants are evaluated with the ANO1 (ANO0) basis set. Anharmonic resonance polyads are treated with the VPT2+K effective Hamiltonian approach. Among the predicted fundamental frequencies, the ground state O−O stretch, excited state O−O stretch, and excited state C−O−O bend fundamentals are predicted at 1138, 959, and 490 cm^{-1}, respectively. Basis set sensitivity is found to be particularly great for the O−O stretches, similar to what has already been noted in smaller, unbranched peroxy radicals. Exempting these O−O stretches, agreement with the available experimental fundamentals is generally good ($\pm$ 10 cm^{-1}).

2 Introduction

Peroxy radicals ($RO_2^{\cdot}$) are integral species to low-temperature oxidation processes that occur in terrestrial combustion environments and in the troposphere. The kinetics of peroxy radical isomerizations often dictate pre-ignition and engine knock events.[1,2] In the atmosphere, the oxidation of alkanes proceeds via hydrogen abstraction by OH, followed by reaction with O_2, forming a peroxy radical intermediate. Peroxy radicals have implications for air quality, as 90% of tropospheric ozone is thought to derive from reactions involving them.[3] Tracking the formation and decomposition of peroxy radicals is thus key to understanding these processes. Of particular utility is the use of species-selective electronic absorptions to monitor the kinetics of specific peroxy radicals.[4]

Early attempts at spectroscopic characterization of peroxy radicals utilized ultraviolet $\widetilde{B} \leftarrow \widetilde{X}$ transitions.[5] Each such transition corresponds to a $\pi \rightarrow \pi^*$ excitation within the C−O−O moiety of most peroxy radicals.[6–8] Increased occupation of the π^* orbital makes the $\widetilde{B}$ state dissociative along the C−O and O−O coordinates.[9–11] As such, these transitions yield largely structureless absorption peaks, which prevent unambiguous assignment to specific R groups of a peroxy radical.

Work on the vibrational spectroscopy of *tert*-butyl peroxy radical remains limited. The earliest bands were identified by Parkes and Donovan.[12,13] They produced *tert*-butyl peroxy radical from photolysis of azoisobutane and subsequently reacted it with molecular oxygen; they observed two gas-phase transitions at 693.7 ± 0.05 cm^{-1} and 760 ± 2 cm^{-1}. Parkes and Donovan argued that these transitions could derive from *tert*-butyl peroxy radical by comparisons to the known vibrational frequencies of other molecules containing a *tert*-butyl group bonded to oxygen. The next development was an argon matrix-isolation study by Chettur and Snelson.[14] They identified nine vibrational transitions in the 200-1200 cm^{-1} range, which they assigned to the O−O stretch (1124 ± 2 cm^{-1}), C−O stretch (730 ± 2 cm^{-1}), and C−C stretches (808 ± 2 cm^{-1}), as well as H−C−H bends (1187 and 1139 ± 2 cm^{-1}) and various skeletal bending vibrations (< 539 cm^{-1}). To aid in these assignments, Chettur and Snelson performed isotopic substitution experiments wherein they deposited a mixture of $^{16}O_2$ and $^{18}O_2$ onto the matrix.

Another attractive spectroscopic approach probes the $\widetilde{A} \leftarrow \widetilde{X}$ vibronic transitions. For alkyl peroxy radicals, these are $n \rightarrow \pi^*$ transitions localized on the the peroxy moiety. Such transitions enabled the observation of excited state O−O stretching progressions of alkyl radicals early on;[15] however, this approach is generally limited by the small $\widetilde{A} \leftarrow \widetilde{X}$ absorption cross-sections, which are 10^4–10^5 times weaker than $\widetilde{B} \leftarrow \widetilde{X}$ transitions.[11] Cavity ringdown spectroscopy (CRDS) alleviates these issues by increasing the effective optical path length.[16–19] The Miller group has reviewed energetic trends in small peroxy radicals by using computational chemistry to supplement and explain their CRDS experiments.[11] They found that branching at the α carbon atom had the most significant effect on the energy of the $\widetilde{A} \leftarrow \widetilde{X}$ electronic transition: tertiary peroxy radicals absorb further to the blue than secondary radicals, which absorb further to the blue than primary radicals.

Glover and Miller[20] employed CRDS to measure the $\widetilde{A} \leftarrow \widetilde{X}$ band of the *tert*-butyl peroxy radical between 7250-8750 cm^{-1}. The peroxy radical was formed via the reaction of O_2 with *tert*-butyl, which was produced from two different sources: chlorine-initiated hydrogen-abstraction

from isobutane and photolysis of *tert*-butyl bromide. They assigned bands at 7757, 8242, and 8695 cm^{-1} to the $\widetilde{A} \leftarrow \widetilde{X}$ band origin and to the simultaneous excitation of one quantum of excited state C−O−O bending and O−O stretching, respectively. The presence of the latter two bands was attributed to favorable Franck-Condon overlap, which results from the large geometric change in the C−O−O moiety where the $\widetilde{A} \leftarrow \widetilde{X}$ transition is localized. They also observed two triplets of bands at (7895, 7994, 8094 cm^{-1}) and (8358, 8476, and 8523 cm^{-1}). They speculated that these bands could correspond to the band origins and the C−O−O bend fundamentals of additional conformers. One plausible way in which this could be achieved is if the three-fold symmetric peroxy torsional potential possesses additional shallower wells capable of supporting bound states. Glover and Miller suggested that the six equivalent points, over the full 360 degree rotation, at which the peroxy group eclipses the hydrogen atom of a methyl group, might correspond to equivalent transition states. The potential would then contain two sets of three equivalent minima. Similar characteristics have been predicted for the CH_2-torsional potential of the *n*-propyl radical; however, the shallower wells disappear after correcting for zero-point energy, leaving the torsional potential with a single minimum at the C_s geometry.[21] As an alternative to the additional conformers hypothesis, they also posited that these triplets could arise from the hindered rotation of the peroxy moiety.

The Miller group soon returned to *tert*-butyl peroxy to answer these lingering questions.[22] Sharp, Rupper, and Miller improved upon their experimental spectrum, refining the frequency of the origin transition to 7755 ± 10 $cm^{-1}$and reported B3LYP/6-31+G* computations of the ground state peroxy torsional potential and ground and excited state harmonic frequencies. Their relaxed torsional potential displayed simple three-fold symmetry, overturning their additional conformers hypothesis. By comparisons to the $\widetilde{A}$ harmonic frequencies, they were able to assign their observed vibrational structure to simultaneous excitation in three low frequency bending degrees of freedom and the O−O stretching degree of freedom. The four fundamentals were assigned at (240, 340, 481, and 934) ± 10 cm^{-1}, respectively. By applying a recommended scaling factor to their harmonic frequencies, their predictions were slightly to the red of the bend fundamentals, but significantly to the blue (24 cm^{-1}) for the O−O stretch fundamental.

Anion photoelectron spectroscopy (APES) was used by Ellison, Lineberger, and co-workers to probe the vibronic states of the peroxy radical.[23,24] In these experiments, *tert*-butyl hydroperoxide [$(CH_3)_3COOH$] was deprotonated by O^- anions, followed by electron detachment via an argon ion

laser. A flow tube surrounded by liquid N_2 was used to cool ions to 200 ± 30 K to reduce rotational broadening. Two peaks were assigned to separate 0_0^0 transitions, allowing for a determination of an $\widetilde{A} \leftarrow \widetilde{X}$ adiabatic electronic excitation energy (T_0) of 7800 ± 90 cm^{-1}. An $\widetilde{X}$ state band at 1130 ± 90 cm^{-1} band was assigned to the O−O stretch through analogy with the HO_2 frequency; this assignment agrees well with the O−O stretch fundamental measured by Chettur and Snelson[14] An $\widetilde{A}$ state band at 930 ± 90 cm^{-1} was also assigned to the O−O stretch. There were also 245 ± 90 cm^{-1} and 240 ± 90 cm^{-1} bands found for the $\widetilde{X}$ and $\widetilde{A}$ states, respectively. These transitions were not assigned to specific vibrations.

Most recently, Neumark and co-workers[25] performed cryo-SEVI photoelectron spectroscopy experiments. In their experiments, $(CH_3)_3COO^-$ anions were guided into a cryogenically cooled octupole ion trap with 20% H_2 in He, wherein the $(CH_3)_3COO^-$ ions were cooled to ~10 K via collisions with the buffer gas. The measured photoelectron spectrum was fit using Franck-Condon simulations that employed B3LYP/6-311+G* scaled vibrational frequencies to compute the Franck-Condon overlap and EOM-IP-CCSD/6-311+G* Dyson orbital computations to determine photodetachment cross sections as functions of the energy. Neumark and co-workers obtained O−O stretch fundamentals of 1129 ± 22 cm^{-1} and 939 ± 14 cm^{-1} for the $\widetilde{X}\ ^2A''$ and $\widetilde{A}\ ^2A'$ electronic states, respectively, which compare favorably to the corresponding values of Chettur and Snelson[14] and Sharp, Rupper, and Miller.[22] They also located the 245 (240) cm^{-1} band for the $\widetilde{X}\ ^2A''$ ($\widetilde{A}\ ^2A'$) state observed by Ellison, Lineberger, and co-workers.[24] They assigned the $\widetilde{X}$ state transition to the ν_{22} fundamental. They did not observe the $\widetilde{A}$ δ(C−O−O) fundamental measured by Sharp, Rupper, and Miller; however, they assigned two new fundamental transitions in the $\widetilde{X}$-state: 279(21) cm^{-1} to ν_{21} and 1254(26) cm^{-1} to ν_{12}. They measured similar energies for the $\widetilde{A} \leftarrow \widetilde{X}$ origin transition as Ellison, Lineberger, and co-workers and Sharp, Rupper, and Miller. Neumark and co-workers did, however, note issues with their B3LYP frequencies, which had to be adjusted at times, so that their Franck-Condon simulations could adequately reproduce their experimental spectra.

Despite decades of careful experimental study, there are still many vibrational fundamentals of the *tert*-butyl peroxy radical that have not been observed. In addition, there is a conspicuous absence of any sophisticated, high-level theoretical treatment that could help confirm these assignments as well as predict the energies of yet-unidentified vibrational transitions. Our group has recently demonstrated the efficacy of extrapolated coupled cluster treatments for predicting the

ground- and first excited state fundamental vibrational transitions for a number of radicals, including the methylperoxy,[26–28] ethylperoxy,[29] propylperoxy,[30] peroxyacetyl,[31] and formylperoxy[32] radicals. This work seeks to expand this success to branched alkyl systems, which have not yet been addressed. We also wish to establish whether current coupled-cluster techniques can be applied to a system of this size and still achieve the same level of accuracy as in our previous research.[33]

3 Theoretical methods

3.1 C−C−O−O torsional potential

To explore the conformational space in the $\widetilde{\mathrm{X}}$ and $\widetilde{\mathrm{A}}$ electronic states, we computed torsional potentials describing the rotation of the peroxy moiety about the C−O bond. To preserve the threefold dynamical symmetry, the scans were carried out in the following way. One of three possible (bonded) C−C−O−O dihedral angles was scanned from 0 degrees (corresponding to the torsional transition state) to 55 degrees, in 5 degree increments. All other internal coordinates, including the other two bonded C−C−O−O dihedral angles, were optimized. Then, at each scan point, the average of the three C−C−O−O angles, τ_{CCOO}, was determined, and this was chosen to represent the true torsional coordinate. A final 60 degree point, corresponding to the equilibrium geometry, was optimized by constraining the in-plane dihedral angle to be 180 degrees while relaxing all other coordinates. The increments of the torsional scan then become only approximately 5 degrees, correcting for the asymmetry introduced by singling out one of three dynamically indistinguishable methyl groups in the original scan.

The geometries were optimized with the CCSD(T) method[34–36] in CFOUR.[37] The 1s-electrons of carbon and oxygen were not correlated in the CCSD(T) computations. An unrestricted Hartree-Fock (UHF) reference wavefunction was used. The atoms were described with the ANO0 truncation (H:[2s1p]; C,O:[3s2p1d]) of the atomic natural orbital (ANO) basis sets of Almlöf and Taylor.[38,39] During optimization, the SCF and CC energies were converged to 10^{-10} E_{h}. At each of the optimized geometries, the electronic energy was refined by performing a CCSD(T) single-point energy computation with the larger ANO1 truncation (H:[4s2p1d]; C,O:[4s3p2d1f]) of the atomic natural orbital (ANO) basis set.[38]

Along most of the peroxy torsional potential, there is no molecular symmetry that can be

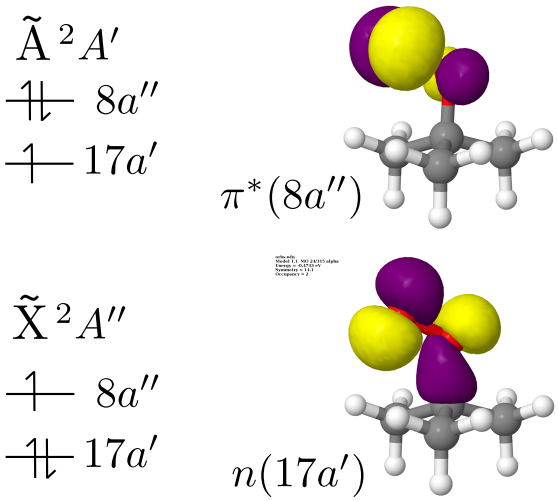

Figure 1: Depiction of the HOMO$_{-1}[n(17a')]$ and HOMO$[\pi^*(8a'')]$ involved in the $\widetilde{\mathrm{A}}\,^2A' \leftarrow \widetilde{\mathrm{X}}\,^2A''$ transition of *tert*-butyl peroxy radical. Shown here are state-averaged CASSCF natural orbitals.

exploited to uniquely target a reference wavefunction for the $\widetilde{\mathrm{A}}$ electronic state, and variational collapse may be a problem. As is the case with all alkylperoxy radicals, the $\widetilde{\mathrm{X}}$ and $\widetilde{\mathrm{A}}$ electronic configurations of *tert*-butyl peroxy radical differ, in zeroth-order, by a simple rotation of two molecular orbitals. For example, the electron configurations at the C_s equilibrium structure of *tert*-butyl peroxy radical can be described as:

$$\widetilde{\mathrm{X}}\,^2A'' : [\mathrm{core}](17a')^2(8a'')^1 \qquad\qquad \widetilde{\mathrm{A}}\,^2A' : [\mathrm{core}](17a')^1(8a'')^2$$

where $17a'$ and $8a''$ are the ground-state HOMO$_{-1}$ and HOMO, respectively. The $17a'$ and $8a''$ orbitals are depicted in Figure 1. The HOMO$_{-1}$ can be thought of as bonding with respect to C−O and nonbonding with respect to O−O, while the HOMO is predominantly antibonding with respect to O−O.[11] In a zeroth-order picture, where $\widetilde{\mathrm{A}} \leftarrow \widetilde{\mathrm{X}}$ excitation does not involve substantial orbital mixing/relaxation, the $\widetilde{\mathrm{A}}$ state simply corresponds to a rotation of these orbitals. In this study we did not find it necessary to rotate the orbitals. Instead we were able to target the excited state wavefunction by using, as a guess at all asymmetric points, the converged orbitals from the nearest symmetric structure.

3.2 $\widetilde{\mathrm{A}} \leftarrow \widetilde{\mathrm{X}}$ Transition origin

The adiabatic $\widetilde{\mathrm{A}} \leftarrow \widetilde{\mathrm{X}}$ excitation energy (T_0) was obtained with the following series of computations. First, we computed the adiabatic $\widetilde{\mathrm{A}} \leftarrow \widetilde{\mathrm{X}}$ electronic transition energy ($T_{e,\mathrm{CBS}}$) via the focal point approach of Allen and co-workers, closely approximating a CCSDT(Q) treatment of electron correlation at the complete basis set (CBS) limit.[40–43] Herein, the relative HF and MP2 energies were computed directly with the cc-pVXZ basis sets[44] up through cc-pVQZ and cc-pV5Z. The relative HF/CBS energy (E^{∞}_{HF}) and MP2/CBS correlation energy ($\epsilon^{\infty}_{\mathrm{MP2}}$) were then obtained by using the values from these latter two basis sets in the two-point extrapolation formulas of Karton and Martin[45] and Helgaker,[46] respectively:

$$E_{\mathrm{HF}}(X) = E^{\infty}_{\mathrm{HF}} + Ae(X+1)e^{-\sqrt{X}}$$
$$\epsilon_{\mathrm{MP2}}(X) = \epsilon^{\infty}_{\mathrm{MP2}} + AX^{-3}.$$

The CCSD and CCSD(T) energies were computed with up to the cc-pVQZ basis set. The cc-pV5Z and CBS values were obtained by assuming additivity; wherein, the CCSD and CCSD(T) increments from cc-pVQZ are assumed to be the same with larger basis sets.

The uncertainty in the electronic energies was assessed by computing the HF and MP2 correlation energies with other extrapolation schemes. Various combinations of HF extrapolations (exp,[47] expGauss,[48] and SchwenkeHF[49]) and correlation energy extrapolations (Schwartz4 and Schwartz6[50]) were tested. Collectively, the $T_{e,\mathrm{CBS}}$ values computed with these combinations had a mean value of 7817 cm^{-1} and a standard deviation of 2 cm^{-1} (see ESI:† Table S1-S13).

Auxiliary corrections were then appended to $T_{e,\mathrm{CBS}}$ to account for certain approximations. We computed the energetic contributions of full-triple and perturbative quadruple excitations using the 6-31G* basis set[51,52] via the following expression:

$$\Delta_{\mathrm{T}} = \Delta E_{\mathrm{CCSDT}} - \Delta E_{\mathrm{CCSD(T)}}$$
$$\Delta_{\mathrm{(Q)}} = \Delta E_{\mathrm{CCSDT(Q)}} - \Delta E_{\mathrm{CCSDT}}$$

A core-correlation correction (Δ_{CORE}) accounts for not correlating the 1s-electrons of carbon and

oxygen:

$$\Delta_{\mathrm{CORE}} = \Delta E_{\text{AE-CCSD(T)}} - \Delta E_{\text{FC-CCSD(T)}}$$

where AE and FC denote the all-electron and frozen-core methods, respectively. The cc-pCVTZ basis set[53] was used. To assess the validity of the separability of the electronic and nuclear coordinates, we computed ROHF/ANO1 diagonal Born-Oppenheimer corrections (Δ_{DBOC}):[54,55]

$$\Delta_{\mathrm{DBOC}} = \langle \Psi_e(r;R) | \hat{T}_N | \Psi_e(r;R) \rangle,$$

where $\Psi_e(r;R)$ is the electronic wavefunction and $\hat{T}_N$ is the nuclear kinetic energy operator. A relativistic correction (Δ_{REL}), including a Darwin term, and one-electron and two-electron mass-velocity terms, accounts for scalar relativistic effects at first-order with direct perturbation theory (DPT):[56,57]

$$\Delta_{\mathrm{REL}} = \Delta E_{\text{AE-CCSD(T)/DPT}} - \Delta E_{\text{AE-CCSD(T)}}.$$

This relativistic correction was evaluated with all-electron CCSD(T)/cc-pCVTZ wavefunctions. Lastly, we appended the relative anharmonic zero-point vibrational energies (Δ_{ZPVE}) to the corrected $T_{e,\mathrm{CBS}}$, which were obtained using the quartic force field described below and a resonance-free expression.[58] In summary, the adiabatic $\widetilde{\mathrm{A}} \leftarrow \widetilde{\mathrm{X}}$ transition energy is expressed fully as:

$$\begin{aligned} T_0 = T_{\mathrm{e,CBS}} + \Delta_{\mathrm{T}} + \Delta_{(\mathrm{Q})} + \Delta_{\mathrm{CORE}} \\ + \Delta_{\mathrm{REL}} + \Delta_{\mathrm{DBOC}} + \Delta_{\mathrm{ZPVE}}. \end{aligned}$$

Using this approach, we obtain a CCSDT(Q)/CBS T_0 value. The incremental nature of the focal point analysis allows us to assess the convergence toward the CBS and full configuration-interaction (FCI) limits as well as the limitations of single-reference, non-relativistic, Born-Oppenheimer wavefunctions. All of the above energy computations employed an ROHF reference. Each energy was converged to within 10^{-10} E_{h}. The Δ_{T} and $\Delta_{(\mathrm{Q})}$ corrections were computed with the Mrcc 2015 program.[59,60] All other energies were computed with CFOUR 1.0. Lastly, we emphasize that all of

the energy computations was performed at the CCSD(T)/ANO1 equilibrium structures described in Section 3.3.

3.3 Anharmonic vibrational frequencies

Anharmonic vibrational frequencies were determined for both the $\widetilde{\mathrm{X}}\ ^2A''$ and $\widetilde{\mathrm{A}}\ ^2A'$ equilibrium structures with second-order vibrational perturbation theory (VPT2),[61] We employed a semi-diagonal quartic force field that includes all force constants up to ϕ_{ijkk} quartic terms. For this research, we constructed a "hybrid" force field where the force constants were computed with the following mixture of levels of theory:

Harmonic Frequencies (ω_i): UHF-CCSD(T)/ANO1
Cubic Force Constants (ϕ_{ijk}): UHF-CCSD(T)/ANO0
Quartic Force Constants (ϕ_{ijkk}): UHF-CCSD(T)/ANO0,

where the indices i, j, k correspond to the normal modes of vibration.

A UHF reference was used throughout to take advantage of the parallelized, analytic CCSD(T) energy derivatives within CFOUR.[62] To obtain all of the force constants, optimized geometries were obtained at the UHF-CCSD(T)/ANO1 and UHF-CCSD(T)/ANO0 levels. Tight convergence parameters were used for all of the optimization and frequency computations described: the SCF densities, CC amplitudes, and Lambda coefficients were converged to $10^{-10}\ E_\mathrm{h}$, and the RMS forces were converged to $10^{-9}\ E_\mathrm{h}\ a_0^{-1}$.

Harmonic vibrational frequencies were obtained by finite differences of UHF-CCSD(T)/ANO1 analytic gradients; harmonic intensities were obtained from finite differences of dipole moments. The cubic and quartic force constants were obtained at the UHF-CCSD(T)/ANO0 level. To obtain these derivatives, displacements were made in the CCSD(T)/ANO0 normal coordinates, and analytic second derivatives were evaluated. Finite differences were then used to obtain the anharmonic force constants.[63]

Anharmonic vibrational frequencies were evaluated via Second-Order Vibrational Perturbation Theory with Resonances (VPT2+K).[64–66] For this research, we employed the diagnostic of Martin, Lee, Taylor, and François[67] to determine if a Fermi Type I ($\omega_i \approx 2\omega_j$) or Type II ($\omega_i \approx \omega_j + \omega_k$) resonance was severe enough to warrant the reduced-dimensional variational treatment (essentially the

+K). We chose the cut-off for stretching and bending modes to be 1 cm^{-1} and elected to not treat stretch-torsion resonances explicitly, as our previous attempts to do this generally worsened agreement with experiment.[68,69] Indeed, this has been recognized by other researchers.[70] The Martin diagnostic is sometimes used in conjunction with simpler energy gap and force constant magnitude tests, with the energy gap test ensuring that stretch-torsion interactions will not be flagged as Fermi resonances.[70] We made one exception to this rule, for a resonance polyad involving ν_{21}, ν_{22}, and $2\nu_{39}$. The diagnostic for the interaction between ν_{21} and $2\nu_{39}$ (161 cm^{-1}) was simply too large to ignore. The resonance diagnostics are given in the Appendix. After being identified, resonances were treated by building and diagonalizing effective Hamiltonians. For these cases, we approximate the anharmonic intensities of the final transitions to be simply fractions of the harmonic intensity of the participating fundamentals, proportional to the squared eigenvector coefficients. In this way, we model the effects of mechanical anharmonicity but not electrical anharmonicity. The Hamiltonian matrices and eigenvectors are given in the ESI:†.

Previous research[26,31,32,71] has found small differences (1–10 cm^{-1}) in harmonic frequencies predicted with a UHF reference, compared with ROHF, due in part to its improper treatment of spin. To correct for these deficiencies, optimized geometries and harmonic vibrational frequencies were also computed at the CCSD(T)/ANO0 level with an ROHF reference. The harmonic vibrational frequencies were then used to compute a small correction:

$$\delta\omega = \omega^{\mathrm{ROHF}}_{\mathrm{CCSD(T)/ANO0}} - \omega^{\mathrm{UHF}}_{\mathrm{CCSD(T)/ANO0}}.$$

This $\delta\omega$ was added to the final anharmonic vibrational frequencies. In the case of resonance polyads, the diagonal values of the effective Hamiltonians were corrected in this manner.

3.4 Reliability of the methods

We checked for substantial deviations of $\langle \hat{S}^2 \rangle_{\mathrm{UHF}}$ from the proper value (0.75 in atomic units). Additionally, the single-reference character of the HF wavefunctions was confirmed by inspecting the squares of the three leading CASCI coefficients from a complete active-space SCF (CASSCF) wavefunction[72,73] that was computed with the ANO1 basis set. The active space consisted of 11 electrons distributed among 6 a' and 6 a'' symmetry orbitals around the HOMO-LUMO gap. These

diagnostics are available in the Appendix (Table 5).

4 Results and discussion

C−C−O−O torsional potential

Figure 2 depicts the C−C−O−O torsional potential for the $\widetilde{\mathrm{X}}$ and $\widetilde{\mathrm{A}}$ electronic states. The shape of the curve illustrates that the potential for peroxy torsion displays simple three-fold symmetry for both electronic states, rather than possessing additional finer structure (including extra wells) akin to *n*-propyl radical's CH_2 torsional potential.[21] The appearance of the torsional potential, in the ground state, is consistent with what was previously computed.[22] Each curve contains maxima at $\tau_{\mathrm{CCOO}} = 0,\ 120^\circ$ that correspond to equivalent structures where the peroxy group is eclipsed with respect to the methyl groups. The minimum of each curve ($\tau_{\mathrm{CCOO}} = 60^\circ$) corresponds to a structure where the peroxy group is staggered with respect to the methyl groups.

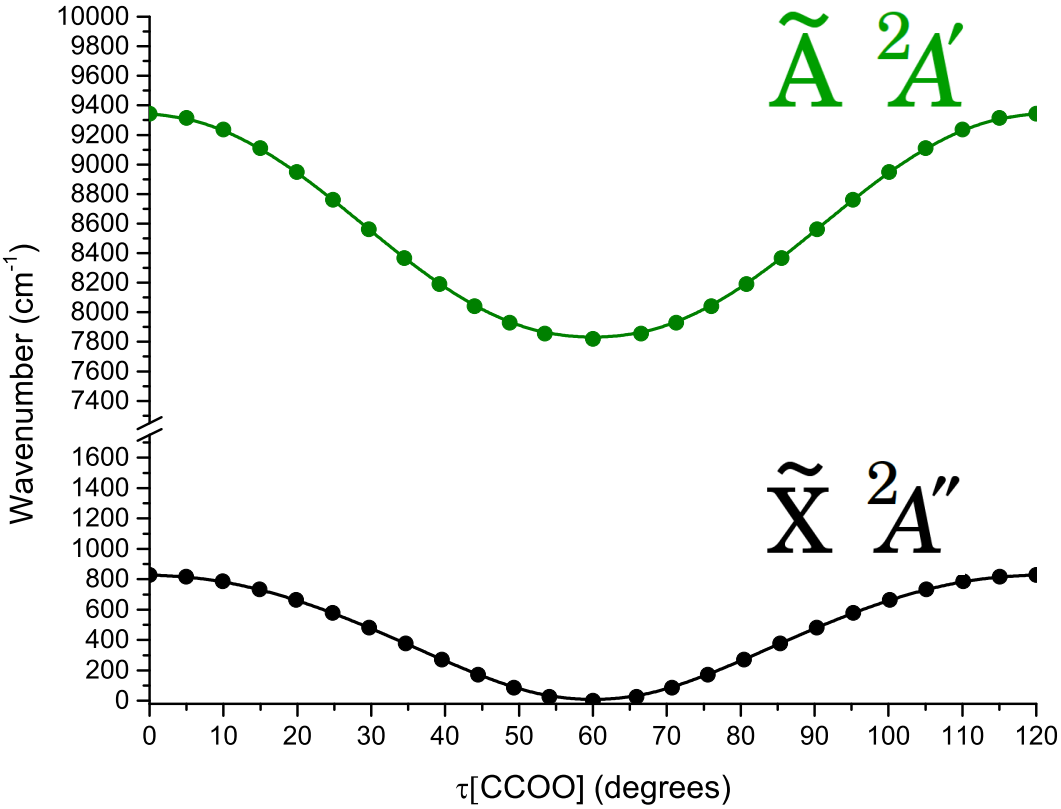

Figure 2: Three-fold symmetric C−C−O−O torsional potentials for the $\widetilde{\mathrm{X}}$ and $\widetilde{\mathrm{A}}$ electronic states obtained at the UHF-CCSD(T)/ANO1//UHF-CCSD(T)/ANO0 level of theory. The $\widetilde{\mathrm{A}}$ energies are offset by the $T_{e,\mathrm{CBS}}$ value from Table 2.

The two potential curves differ in the height of the peroxy torsion barrier, which is 828 cm^{-1} and 1523 cm^{-1} in the $\widetilde{\mathrm{X}}$ and $\widetilde{\mathrm{A}}$ electronic states, respectively. Launder *et al.*[29] computed peroxy torsional potentials for the $\widetilde{\mathrm{X}}$ and $\widetilde{\mathrm{A}}$ states of the ethyl peroxy radical. These are similar in that the barriers for the $\widetilde{\mathrm{A}}$ state are also about twice as high as those for the $\widetilde{\mathrm{X}}$ state. Note that the torsional potential of ethyl peroxy radical possesses lower symmetry; it displays two distinct conformers.

They found that the torsional transition states corresponded to structures where the peroxy moiety eclipsed some other part of the molecule (either the β-methyl group or the α-hydrogen). Additionally, they also predicted the peroxy torsional barrier to be much steeper in the $\widetilde{\mathrm{A}}$ state. Similar trends in computed torsional potentials were also found by Miller and co-workers for other peroxy radicals, including: methyl, allyl and cyclopentadienyl peroxy.[74–76]

For the methyl peroxy radical, Just, McCoy, and Miller explain the higher barriers in the excited state based upon destabilization of the HOMO[$\pi^*(a'')$].[74] They argue that, when the per-

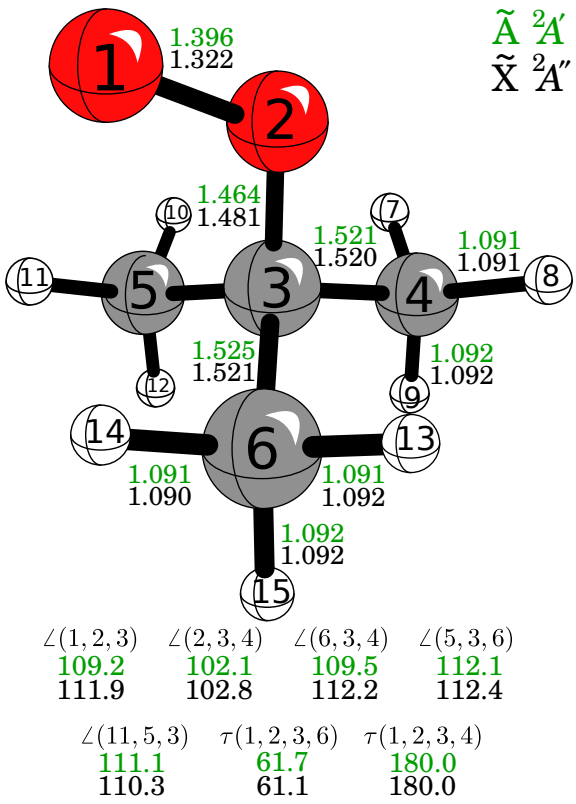

Figure 3: Optimized equilibrium structure for the $\tilde{X}\ ^2A''$ and $\tilde{A}\ ^2A'$ electronic states of the *tert*-butyl peroxy radical obtained at the UHF-CCSD(T)/ANO1 level of theory. The bond distances are in angstroms, and the angles are in degrees.

oxy radical is in a staggered orientation, the HOMO[$\pi^*(a'')$] experiences favorable delocalization (*i.e.* hyperconjugation) over the adjacent C−H bonds; however, this delocalization is mostly lost when it assumes an eclipsed orientation. The energy stabilization should be enhanced when the HOMO[$\pi^*(a'')$] is doubly-occupied, as it is in the $\tilde{A}$ state. Miller and co-workers also note that the HOMO$_{-1}$[$n(a')$] and other orbitals of a' symmetry do not noticeably change from one orientation to the other. Similar arguments also apply to *tert*-butyl peroxy; however, in the staggered configuration, its HOMO[$\pi^*(8a'')$] is delocalized over the adjacent C−C bonds. In the $\tilde{A}$ state, the decreased occupation of the HOMO$_{-1}$[$n(17a')$] also decreases the length of the C−O bond, and the C−O bond has to elongate more along the potential in the $\tilde{A}$ state, in response to repulsion from the methyl groups. From the bottom of the well to the top of the barrier, the C−O bond elongates by 0.009 and 0.019 Å for the $\tilde{X}$ and $\tilde{A}$ states, respectively.

Equilibrium structures

Figure 3 depicts the UHF-CCSD(T)/ANO1 equilibrium structure of the *tert*-butyl peroxy radical, with select geometrical parameters, for the $\widetilde{\mathrm{X}}\ ^2A''$ and $\widetilde{\mathrm{A}}\ ^2A'$ electronic states. For both states, the peroxy moiety is staggered with respect to the methyl groups. The $\widetilde{\mathrm{A}}\ ^2A' \leftarrow \widetilde{\mathrm{X}}\ ^2A''$ transition (Figure 1) primarily involves the excitation of a single electron from the HOMO$_{-1}[n(17a')]$ to the HOMO$[\pi^*(8a'')]$, which are localized on the peroxy moiety. As such, this transition only induces significant changes in the C−O and O−O bonds. The $\widetilde{\mathrm{A}} \leftarrow \widetilde{\mathrm{X}}$ transition induces an elongation of the O−O bond ($\Delta r_\mathrm{e} = 0.074$ Å) and contraction of the C−O bond ($\Delta r_\mathrm{e} = -0.017$ Å). In contrast, the C−C bond lengths shift only very slightly: the in-plane C−C bond and out-of-plane C−C bonds elongate by only 0.004 Å and 0.001 Å, respectively. These structural changes induced by the $\widetilde{\mathrm{A}} \leftarrow \widetilde{\mathrm{X}}$ excitation are remarkably similar to those computed for the methyl peroxy[26] and ethyl peroxy[29] radicals, as shown in Table 1. It is also noteworthy that the 6-3-4 C−C−C angle and the C−O−O angle both contract by 2.7 degrees upon excitation.

Energetic trends of peroxy radical conformers have already been discussed in the article by Sharp, Rupper, and Miller.[11] Some discussion was also devoted to geometric trends. They argue that the hyperconjugating effect is weakened in peroxy radicals that are branched at the carbon atom adjacent to the peroxy group. They show that the SOMO (in the ground electronic state) of primary peroxy radicals is delocalized over the nearby CH bonds; however, in secondary and tertiary peroxy radicals, the SOMO is more localized on the peroxy moiety. Miller and co-workers expected that this hyperconjugation should stabilize the C−O bond. The greater lengthening of the C−O bond that we find in *tert*-butyl peroxy versus the primary peroxy radicals is consistent with the arguments put forth by Sharp *et. al.*[11]

$\widetilde{\mathrm{A}} \leftarrow \widetilde{\mathrm{X}}$ Transition origin

The CBS extrapolation and the auxiliary corrections used to obtain the adiabatic $\widetilde{\mathrm{A}} \leftarrow \widetilde{\mathrm{X}}$ excitation energy (T_0) are given in Table 2. We predict a T_0 value of 7738 cm^{-1}. The difference between the CCSD(T) energies with the cc-pVQZ and CBS limits shows good convergence with respect to the basis set. The sum of the post-CCSD(T) corrections (47 cm^{-1}) is very close to the analogous correction determined for the methyl peroxy radical (56 cm^{-1}).[26] This is promising since Copan *et al.*

Table 1: Comparison of predicted geometric parameters, transition energies, and vibrational frequencies for the *tert*-butyl peroxy radical, ethyl peroxy radical, and methyl peroxy radical. In all cases, geometries were optimized with the CCSD(T) method and a basis set of at least triple zeta quality. Transition energies were evaluated with Focal Point Analysis (FPA).

Parameter[a]	*tert*-butyl	*gauche*-ethyl[29]	*trans*-ethyl[29]	methyl[26]
Δr_e(C−O)	−0.017	−0.012	−0.012	−0.012
Δr_e(O−O)	+0.074	+0.073	+0.074	+0.075
Δa_e(C−O−O)	−2.7	−3.6	−4.7	−4.8
T_0	7738	7583	7363	7374
$\widetilde{\mathrm{X}}$:ν(O−O)	1138	1123	1152	1186, 1128
$\widetilde{\mathrm{A}}$:ν(O−O)	959	···	···	1008, 910
$\widetilde{\mathrm{X}}$:δ(C−O−O)	541	529	500	493
$\widetilde{\mathrm{A}}$:δ(C−O−O)	490	···	···	379

[a] Distances in Å, angles in degrees, T_0 in cm^{-1}, and frequencies in cm^{-1}.

computed that the difference between perturbative and full quadruples was only ∼10 cm^{-1} in methyl peroxy. It is important to question whether a good quality prediction of the $\widetilde{\mathrm{A}} \leftarrow \widetilde{\mathrm{X}}$ origin can be achieved using an ANO0 optimized geometry. At the CCSD(T)/cc-pVQZ//CCSD(T)/ANO0 level, we calculate a T_e value of 7828 cm^{-1}, which differs somewhat from the 7792 cm^{-1} T_e value obtained at the CCSD(T)/ANO1 geometry.

Table 1 shows that the T_0 of *tert*-butyl peroxy radical (7738 cm^{-1}) is appreciably greater than T_0 of the ethyl peroxy (*gauche*: 7583 cm^{-1}, *trans*: 7363 cm^{-1})[29] and methyl peroxy radicals (7374 cm^{-1}),[26] which highlights the utility of these $\widetilde{\mathrm{A}} \leftarrow \widetilde{\mathrm{X}}$ transitions for specific identification of peroxy radicals. Sharp, Rupper, and Miller previously explored these trends, concluding that α-branching induced the greatest blueshift to T_0, followed by gauche orientation of τ_{CCOO}.

We now compare our predicted T_0 value (7738 cm^{-1}) to previous experimental values. We observe excellent agreement with the available experimental values from Sharp, Rupper, and Miller (7755 ± 10 cm^{-1})[22] and Neumark and co-workers (7744 ± 19 cm^{-1}).[25] Our value also falls well within the error bars of the value from Ellison, Lineberger, and co-workers (7799 ± 90 cm^{-1})[24]. To the best of our knowledge, the only other attempt to compute T_0 was performed by Neumark and co-workers, who predicted this energy to be 7933 cm^{-1} at the B3LYP/6-311+G* level of theory. The excitation energy cannot be predicted accurately by DFT (and without considering, at minimum, the effect of core-valence correlation). Our higher level determination signals a coalescence of theory and experiment regarding the energy of the $\widetilde{\mathrm{A}} \leftarrow \widetilde{\mathrm{X}}$ origin transition and shows that accuracy

approaching the best quality experimental measurements may indeed be achieved for larger peroxy radicals.

Table 2: The adiabatic $\widetilde{\mathrm{A}} \leftarrow \widetilde{\mathrm{X}}$ origin transition energy (T_0), obtained at the CCSDT(Q)/CBS//CCSD(T)/ANO1 level. Bracketed values were obtained by additivity or extrapolation assumptions. All energies are in cm^{-1}.

	ROHF	$+\delta$MP2	$+\delta$CCSD	$+\delta$CCSD(T)	NET
cc-pVDZ	4687	+2529	+87	+201	7503
cc-pVTZ	4732	+2570	+71	+311	7684
cc-pVQZ	4758	+2614	+86	+334	7792
cc-pV5Z	4758	+2628	[+86]	[+334]	7805
CBS LIMIT	[4758]	[+2643]	[+86]	[+334]	**7820**

$$T_0 = T_{e,\mathrm{CBS}} + \Delta_{\mathrm{T}} + \Delta_{(\mathrm{Q})} + \Delta_{\mathrm{CORE}} + \Delta_{\mathrm{DBOC}} + \Delta_{\mathrm{REL}} + \Delta_{\mathrm{ZPVE}}$$
$$T_0 = 7820 - 0.6 + 47.5 + 23.5 + 0.5 - 5.1 - 147.3 \ \mathrm{cm}^{-1}$$
$$T_0 = \mathbf{7738\ cm^{-1}}$$

Fundamental vibrational frequencies

Assessing the quality of the force field

One potential shortcoming of our force field is the use of a UHF reference determinant, which does not properly handle spin, for the cubic and quartic force constants. Table 5 in the Appendix shows that the UHF reference is only minimally spin-contaminated, so we should not expect significant errors in the vibrational frequencies due to this. Indeed, this is largely the case when we consider the $\delta\omega$ corrections obtained with the ROHF reference. Nearly all corrections are less than 1 cm^{-1}. The more substantial corrections are tabulated in the Appendix (Table 6). The most notable of these are for the O−O stretch in the $\widetilde{\mathrm{X}}$ state (ν_{13}) and $\widetilde{\mathrm{A}}$ state (ν_{14}), which amount to -4 cm^{-1} and -18 cm^{-1}, respectively. While these corrections largely align with similar corrections in previous research,[26,31,32,71] the $\widetilde{\mathrm{A}}$ state is particularly large; this may result from its slightly higher spin contamination. However, it is not surprising that only modes involving the C−O−O moiety are greatly affected, because the spin density is largely localized there. Finally we note that differences in force constants, based upon different reference wavefunctions, can also be due to orbital near-instabilities (in the references).[77] This is more frequently a concern in systems that

possess double- and triple-bonds; however, we cannot completely rule this out as an explanation for these differences.

Other issues may arise from our combination of CCSD(T)/ANO1 quadratic and CCSD(T)/ANO0 cubic/quartic force constants. A central assumption made in most hybrid force fields is that the normal modes do not differ between the two levels of theory (in this case the different basis sets). The extent to which this condition is met depends strongly upon the type of normal coordinate; moreover, this approximation is generally less sound for larger molecules with lower symmetry. Changes in the potential energy surface, at different levels of theory, will influence how the internal coordinates couple together into normal coordinates. We have found that the O−O and C−O stretch coordinates of peroxy radicals are particularly sensitive to the level of theory and basis set size. These oscillators have similar masses; depending on the potential, they may remain decoupled, or they may couple into symmetric and antisymmetric C−O−O stretch normal coordinates. By visual inspection of the normal mode displacements, the extent of coupling between the two stretches changes between the different levels of theory; this occurs to a greater extent in the $\widetilde{\mathrm{A}}$ state.

For the ethyl peroxy radical, we recently showed that transformation of the cubic/quartic force constants into the same normal coordinates as the quadratic force constants makes them very closely approximate the values of the analogous force constants at a higher level of theory.[78] This suggests that the normal-mode mismatching is largely responsible for the disagreement between force constants computed at different levels of theory. Despite its general success, the aforementioned transformation did not improve the agreement for the O−O stretching force constants. This degree of freedom, in addition to being impacted by the normal-mode mismatching, evidently requires a more complete basis set than ANO0 to describe accurately.[4] Both of these factors are implicated in the lower accuracy predictions of the O−O stretch fundamentals for the *tert*-butyl peroxy radical; unfortunately, the necessary corrections were deemed too expensive for this (15-atom) system. As a follow-up, we feel that it would be of great practical value to conduct a dedicated study of O−O stretch transitions of peroxy radicals, in order to evaluate their sensitivity to various aspects of the one-electron basis set (diffuse functions, high angular momentum functions), reference wavefunction (UHF vs. ROHF vs. Brueckner), correlation treatment (core-correlation, post-CCSD(T) correlation), and anharmonicity treatment (empirical scaling vs. VPT2).

Fermi resonances

Using the threshold described in the methods section, several Type I and Type II Fermi resonances were identified. Resonances with diagnostic values exceeding the threshold are given in the Appendix (Table 7). The Fermi resonances are primarily isolated in the C−H stretching (3145–3044 cm^{-1}) and H−C−H bending regions (1523–1400 cm^{-1}). The only exception is a Fermi triad involving the ν_{21}, ν_{22}, and $2\nu_{39}$ states in the $\widetilde{X}$ electronic state. These are both regions for which there is presently no experimental information. As seen in the Appendix (Table 7), there are several vibrational states that strongly interact. The variational mixing between deperturbed vibrational states is sometimes as high as 50/50, resulting in vibrational states that can no longer be correlated with any zeroth-order harmonic oscillator states. Several large resonance polyads exist in the $\widetilde{X}$ state, as the C−H stretching states are sometimes in resonance with doubly-excited H−C−H bending states, and these are, in turn, in resonance with even more highly-excited low-frequency bending states.

Comparison to previous research

Six previous experimental studies[12,14,20,22,24,25] have measured bands of the *tert*-butyl peroxy radical. In total, fifteen distinct fundamental transitions have been assigned. Eleven of these transitions are associated with the $\widetilde{X}$ state and four with the $\widetilde{A}$ state. Our predictions for the fundamental transitions of the $\widetilde{X}$ and $\widetilde{A}$ states are listed in Tables 3 and 4, respectively. When there is a consensus between the assignments of theory and experiment, and exempting the pathological O−O stretches, there is good agreement with the predicted frequencies ($\pm$ 10 cm^{-1}). Regarding our calculated intensities, recall that these are infrared absorption intensities based upon geometric derivatives of the dipole moment; as such, these can only be meaningfully compared to the infrared absorption experiments. The mechanism that gives rise to transition intensity in the CRDS experiment[20,22] is, instead, favorable Franck-Condon overlap between the ground and excited state vibrational wavefunctions. Similarly, the active vibrations in the APES experiments[24,25] are those with favorable overlap between the closed shell anion and either the ground or the excited state of the neutral radical.

Comparison to $\widetilde{\mathrm{X}}\ ^2A''$ fundamental transitions from experiment

The most recent experiment from Neumark and co-workers[25] observed six fundamental vibrations for the $\widetilde{\mathrm{X}}$ state. Three fundamentals can readily be compared to our predicted values: ν_{13}, ν_{17}, and ν_{19}. We predict frequencies for these transitions of 1138, 737, and 401 cm^{-1}, which agree with the 1129, 740, and 410 cm^{-1} values observed in the experiment. Note however that the fundamental at 740 cm^{-1} was not directly observed; rather, it was estimated by subtracting the value of ν_{13} from a combination band assigned as $\nu_{13}+\nu_{17}$. It should, therefore, not be considered as accurate as the others. Chettur and Snelson[14] measured similar bands at 1124, 730, and 403 cm^{-1}, which they attributed to O−O stretching, C−O stretching, and skeletal bending, respectively. Their assignments, based off isotopic shifts, align well with the amount of oxygen motion that occurs in ν_{13}, ν_{17}, and ν_{19}. Therefore, theory and experiment appear to align nicely for these three fundamental transitions. The slight red shifts of the frequencies of Chettur and Snelson are consistent with typical argon matrix perturbations.

Neumark and co-workers also reported vibrational bands at 236 cm^{-1} and 279 cm^{-1}, which they assigned to ν_{21} and ν_{22}, respectively. These values nearly match two of the frequencies of the $\nu_{21}/\nu_{22}/2\nu_{39}$ Fermi triad: 229, 247, and 275 cm^{-1}. The 236 cm^{-1} also matches our predicted value for ν_{37} of 236 cm^{-1}; however, this vibration is antisymmetric and is unlikely to be active in their experiment. As noted by Neumark and co-workers[25], their 236 cm^{-1} band may correspond with the 245 cm^{-1} band measured by Lineberger, Ellison, and co-workers.[24]

The last $\widetilde{\mathrm{X}}$ vibrational transition reported by Neumark and co-workers was at 1254 cm^{-1}, which they assigned to the CC_3 symmetric bend (*i.e.* skeletal umbrella) fundamental (ν_{12}). As with ν_{17}, the value of this fundamental was estimated from a combination band which they assigned as $\nu_{12}+\nu_{13}$. According to our calculations, it is more likely that the combination band corresponds to $\nu_{11}+\nu_{13}$, and their fundamental should instead be considered an estimate of the a' CC_3 antisymmetric bend fundamental, ν_{11}, which we predict at 1269 cm^{-1}. The only observation of ν_{12} appears to be by Chettur and Snelson[14] at 1187 cm^{-1}. This agrees much better with our prediction (1190 cm^{-1}) for the CC_3 symmetric bend fundamental. To corroborate this, we predict $\nu_{12}+\nu_{13}$ at 2326 cm^{-1} and $\nu_{11}+\nu_{13}$ at 2405 cm^{-1}; Neumark and co-workers' experimental band at 2382 cm^{-1} agrees better with the latter.

The last set of measured $\widetilde{\mathrm{X}}$ bands were those from Chettur and Snelson, corresponding to various bends and stretches below 1000 cm^{-1}. We find, for each experimental band, a predicted frequency in close agreement (Table 3). Moreover, the isotopic shifts are consistent with the amount of O−O motion in each normal mode.[14]

Comparison to $\widetilde{\mathrm{A}}\ ^2A'$ fundamental transitions from experiment

Neumark and co-workers[25] also measured $\widetilde{\mathrm{A}}$ -state fundamentals. They found, for the O−O stretch, a frequency of 939 ± 14 cm^{-1}, in excellent agreement with the 934 ± 10 cm^{-1} reported by Sharp, Rupper, and Miller.[22] Our prediction of 959 cm^{-1} deviates somewhat from these. We have already discussed the difficulties associated with accurately modeling the O−O stretching degree of freedom.

This transition represents the most significant disagreement between our predicted values and experiment. Notably, similar issues have been observed for the methyl and ethyl peroxy radicals, despite their relative simplicity and treatments with higher levels of theory. For the methyl peroxy radical, normal mode analysis does not predict a localized O−O stretch, but the predicted values of the $\widetilde{\mathrm{A}}$ symmetric and antisymmetric C−O−O stretches deviate from gas-phase measurements by 12 cm^{-1} and 14 cm^{-1}, respectively. For the ethyl peroxy radical, the $\widetilde{\mathrm{X}}$ -state O−O stretch deviates by at least 11 cm^{-1} (assignment of O−O is ambiguous) from the gas phase value. This is unfortunate, as the O−O stretch is among the most easily measured transitions for the $\widetilde{\mathrm{X}}$ and $\widetilde{\mathrm{A}}$ states due to its high Franck-Condon activity (in both direct vibronic absorption and anion photoelectron spectroscopies). Additionally, it is sensitive to the peroxy radical R-group and can serve as another valuable identification aid (in addition to the band origin).

Sharp, Rupper, and Miller also assigned a transition at 481 ± 10 cm^{-1} to the $\widetilde{\mathrm{A}}$-state C−O−O bending fundamental.[22] For this, we find good agreement with our predicted ν_{18} fundamental of 490 cm^{-1}. This mode is reasonably described as C−O−O bending. At 340 ± 10 cm^{-1} they assigned a band as CCC bending; this agrees with our prediction of 347 cm^{-1}.

The only other measured $\widetilde{\mathrm{A}}$ transitions were 244 cm^{-1} from Neumark and co-workers[25] and two 240 cm^{-1} bands from Sharp, Rupper, and Miller[22] and Lineberger, Ellison, and co-workers.[24] Neumark and co-workers did not offer a definitive assignment for their band; they stated that either ν_{21} or ν_{22} was reasonable based on their Franck-Condon simulations. Our theory is also not conclusive; while there is not a strongly interacting Fermi triad in this range (as in the $\widetilde{\mathrm{X}}$

state), our predicted ν_{21}, ν_{22}, and ν_{37} frequencies all are in good agreement with this mode. We find assignment to ν_{37} less likely since it is an antisymmetric vibration.[22] These two bands do not necessarily have to correspond to the same transition, as the two types of experiments do not light up exactly the same vibrations. Hence, in agreement with Neumark and co-workers, we would assign these two observed transitions to either ν_{21} or ν_{22}.

Experimental bands with no clear assignments

Parkes and Donovan[12] measured the first infrared spectrum of the *tert*-butyl peroxy radical in the gas phase. They observed two bands at 693 ± 1 and 760 ± 2 cm^{-1}. Neither of these transitions align with our predicted vibrational fundamentals or with bands measured in subsequent experiments. Our prediction for ν_{17} (at 737 cm^{-1}) comes closest to the latter band; however, the respective 740 $\pm$ 26 cm^{-1} and 730 $\pm$ 2 cm^{-1} bands of Neumark and co-workers[25] and Chettur and Snelson,[14] taken with the theoretical predictions of this research, make Parkes and Donovan's assignment of this band to *tert*-butyl peroxy tenuous. It is possible that the bands instead belong to the product of the photolysis + oxidation process carried out on azoisobutane.

Lastly, we discuss an $\widetilde{\mathrm{X}}$ band at 1139 cm^{-1} measured by Chettur and Snelson. This value *only* aligns with our predicted 1138 cm^{-1} frequency for the O−O stretch; however, as discussed earlier, we agree with the conclusions of Chettur and Snelson that their 1124 cm^{-1} band corresponds to the O−O stretch. This is most clearly seen by the isotopic shifts Chettur and Snelson measured for the 1139 cm^{-1} and 1124 cm^{-1} bands. Upon $^{18}O_2$ substitution, the 1139 cm^{-1} shifts by only 2 cm^{-1}, while the 1124 cm^{-1} band shifts by 54 cm^{-1}. Unfortunately, this makes one wonder exactly what the 1138 cm^{-1} band corresponds to. An intense combination or overtone band is the first reasonable guess; however, there are many theoretical possibilities that could explain this, and assigning a certain combination or overtone transition is not possible, given the data.

Table 3: Fundamental vibrational frequencies (ν) for the $\widetilde{\mathrm{X}}\ ^2A''$ state of the *tert*-butyl peroxy radical. All theoretical results are from the present research.

	Mode[a]	Theory			Expt.[d]		
		ω[b]	ν[c]	Int.[b]	Ref. 25[f]	Ref. 24[f]	Ref. 14[g]
a'							
ν_1	$\nu_{as}(CH_3)_2$	3145	2996	14.9	···	···	···
ν_2	$\nu_{as}(CH_3)_3$	3132	2985	29.5	···	···	···
ν_3	$\nu_{as}(CH_3)_3$	3125	2978	3.6	···	···	···
ν_4	$\nu_s(CH_3)_3$	3049	2930, 2970	6.6, 1.1	···	···	···
ν_5	$\nu_s(CH_3)_3$	3044	2908, 2953	4.2, 3.7	···	···	···
ν_6	$\delta_{as}(CH_3)_3$	1523	1482	10.5	···	···	···
ν_7	$\delta_{as}(CH_3)_2$	1500	1454, 1469	1.8, 1.8	···	···	···
ν_8	$\delta_{as}(CH_3)_3$	1489	1449, 1454	0.2, 1.8	···	···	···
ν_9	$\delta_s(CH_3)_3$	1423	1391	6.2	···	···	···
ν_{10}	$\delta_s(CH_3)_3$	1402	1361, 1369	1.7, 21.8	···	···	···
ν_{11}	$\delta_{as}(CC_3)$	1308	1269	11.9	1254 ± 26[e]	···	···
ν_{12}	$\delta_s(CC_3)$	1221	1190	26.4	···	···	1187 ± 2
ν_{13}	ν(OO)	1167	1138	18.1	1129 ± 22	1130 ± 90	1124 ± 2
ν_{14}	$\rho_r(CH_3)_3$	1056	1031	0.3	···	···	···
ν_{15}	ν_{as}(CC)	938	920	0.6	···	···	···
ν_{16}	ν_{as}(CC/CO)	853	823	6.8	···	···	808 ± 2
ν_{17}	ν_s(CC/CO)	751	737	1.8	740 ± 26[e]	···	730 ± 2
ν_{18}	δ(COO)	549	541	6.3	···	···	539 ± 2
ν_{19}	δ_{as}(CCC)	399	401	0.5	410 ± 29	···	403 ± 2
ν_{20}	δ(CCO/COO)	361	358	2.4	···	···	361 ± 2
ν_{21}	δ(COO/CCO)	273	229, 247, 275	0.2, 0.2, 1.5	279 ± 21	···	···
ν_{22}	$\tau(CH_3)_2$	254	229, 247, 275	0.2, 0.2, 1.5	236 ± 21	245 ± 90	···
a''							
ν_{23}	$\nu_{as}(CH_3)_2$	3141	2993	3.4	···	···	···
ν_{24}	$\nu_{as}(CH_3)$	3131	2983	19.5	···	···	···
ν_{25}	$\nu_{as}(CH_3)_2$	3123	2977	3.8	···	···	···
ν_{26}	$\nu_s(CH_3)_2$	3045	2906, 2943, 2962	6.7, 2.7, 2.8	···	···	···
ν_{27}	$\delta_{as}(CH_3)$	1499	1460, 1475	0.4, 2.9	···	···	···
ν_{28}	$\delta_{as}(CH_3)_3$	1490	1445, 1460	0.0, 0.4	···	···	···
ν_{29}	$\delta_{as}(CH_3)_3$	1471	1432	0.0	···	···	···
ν_{30}	$\delta_s(CH_3)_2$	1398	1365	19.0	···	···	···
ν_{31}	$\delta_{as}(CC_3)$	1280	1245	12.2	···	···	···
ν_{32}	$\rho_r(CH_3)_3$	1045	1020	0.4	···	···	···
ν_{33}	$\rho_r(CH_3)_3$	965	949	0.0	···	···	···
ν_{34}	ν_{as}(CC)	936	919	0.2	···	···	···
ν_{35}	δ(COO)	438	434	3.1	···	···	···
ν_{36}	δ_{as}(CCC)	333	333	1.1	···	···	337 ± 2
ν_{37}	$\tau(CH_3)_3$	248	236	0.0	···	···	···
ν_{38}	$\tau(CH_3)_3$	191	185	0.0	···	···	···
ν_{39}	τ(CCOO)	127	122	0.2	···	···	···

[a] A qualitative description of each ANO1 normal coordinate is given. Abbreviations used: ν: stretch, δ: deformation, ρ_r: rock, τ: torsion, s: symmetric, as: antisymmetric

[b] Computed at UHF-CCSD(T)/ANO1 level of theory

[c] For participants in a resonance polyad, transitions comprised of greater than 10% of fundamental character are shown here (see ESI:† for details)

[d] Unclear assignments: 1139 cm^{-1} $[\delta(CH_3)]$ [14]

[e] Estimated from a measured overtone or a combination transition

[f] Gas phase, anion photoelectron spectroscopy

[g] Argon matrix, infrared absorption spectroscopy

Table 4: Fundamental vibrational frequencies (ν) for the $\widetilde{\mathrm{A}}\ ^2A'$ state of the *tert*-butyl peroxy radical. All theoretical results are from the present research.

	Mode[a]	Theory			Expt.		
		ω[b]	ν[c]	Int.[b]	Ref. 25[e]	Ref. 24[e]	Ref. 22[f]
a'							
ν_1	$\nu_{as}(CH_3)_2$	3138	2990	21.8	···	···	···
ν_2	$\nu_{as}(CH_3)_3$	3133	2986	28.4	···	···	···
ν_3	$\nu_{as}(CH_3)_3$	3126	2979	7.0	···	···	···
ν_4	$\nu_s(CH_3)_3$	3049	2930, 2970	6.0, 1.3	···	···	···
ν_5	$\nu_s(CH_3)_3$	3045	2909, 2953	5.1, 5.0	···	···	···
ν_6	$\delta_{as}(CH_3)_3$	1521	1483	7.5	···	···	···
ν_7	$\delta_{as}(CH_3)_2$	1499	1462	5.1	···	···	···
ν_8	$\delta_{as}(CH_3)_3$	1488	1452	0.0	···	···	···
ν_9	$\delta_s(CH_3)_3$	1424	1390	8.9	···	···	···
ν_{10}	$\delta_s(CH_3)$	1401	1368	18.0	···	···	···
ν_{11}	$\delta_{as}(CC_3)$	1297	1257	9.5	···	···	···
ν_{12}	$\delta_s(CC_3)$	1215	1182	59.2	···	···	···
ν_{13}	$\rho_r(CH_3)_3$	1051	1026	0.4	···	···	···
ν_{14}	ν(OO)	969	959	33.6	939 ± 14	···	934 ± 10
ν_{15}	ν_{as}(CC)	934	919	4.2	···	···	···
ν_{16}	ν_{as}(CC/CO)	864	842	24.1	···	···	···
ν_{17}	ν_s(CC/CO)	740	727	6.9	···	···	···
ν_{18}	δ(COO)	495	490	4.8	···	···	481 ± 10
ν_{19}	δ(CCO)	403	405	0.6	···	···	···
ν_{20}	δ_{as}(CCC)	347	347	1.7	···	···	340 ± 10
ν_{21}	δ(COO/CCO)	254	252	1.0	244 ± 15[d]	240 ± 90[d]	240 ± 10[d]
ν_{22}	$\tau(CH_3)_2$	250	239	0.7	244 ± 15[d]	240 ± 90[d]	240 ± 10[d]
a''							
ν_{23}	$\nu_{as}(CH_3)_3$	3137	2989	24.1	···	···	···
ν_{24}	$\nu_{as}(CH_3)_3$	3133	2985	0.0	···	···	···
ν_{25}	$\nu_{as}(CH_3)_2$	3123	2977	2.5	···	···	···
ν_{26}	$\nu_s(CH_3)_2$	3043	2910, 2951	5.4, 5.6	···	···	···
ν_{27}	$\delta_{as}(CH_3)_3$	1498	1461	2.4	···	···	···
ν_{28}	$\delta_{as}(CH_3)_2$	1487	1451	0.1	···	···	···
ν_{29}	$\delta_{as}(CH_3)_3$	1470	1435	0.1	···	···	···
ν_{30}	$\delta_s(CH_3)_2$	1403	1369	20.3	···	···	···
ν_{31}	$\delta_{as}(CC_3)$	1283	1249	15.9	···	···	···
ν_{32}	$\rho_r(CH_3)_3$	1050	1024	0.9	···	···	···
ν_{33}	$\rho_r(CH_3)_3$	964	947	0.0	···	···	···
ν_{34}	ν_{as}(CC)	927	909	0.0	···	···	···
ν_{35}	δ(COO)	457	456	4.1	···	···	···
ν_{36}	δ_{as}(CCC)	338	337	1.0	···	···	···
ν_{37}	$\tau(CH_3)_3$	255	243	0.0	···	···	···
ν_{38}	$\tau(CH_3)_3$	197	191	0.0	···	···	···
ν_{39}	τ(CCOO)	112	118	0.1	···	···	···

[a] A qualitative description of each ANO1 normal coordinate is given. Abbreviations used: ν: stretch, δ: deformation, ρ_r: rock, τ: torsion, s: symmetric, as: antisymmetric

[b] Computed at UHF-CCSD(T)/ANO1 level of theory

[c] For participants in a resonance polyad, transitions comprised of greater than 10% of fundamental character are shown here (see ESI:† for details)

[d] Indicates several reasonable assignments

[e] Gas phase, anion photoelectron spectroscopy

[f] Gas phase, cavity ringdown spectroscopy

5 Conclusions

High accuracy theoretical predictions have been made for the fundamental vibrational transitions of the $\widetilde{\mathrm{X}}\,^2A''$ and $\widetilde{\mathrm{A}}\,^2A'$ electronic states of *tert*-butyl peroxy radical. A UHF-CCSD(T)/ANO1//UHF-CCSD(T)/ANO0 peroxy torsional potential shows three equivalent minima for both electronic states, in which the peroxy moiety is staggered with respect to the methyl groups. An eclipsed structure corresponds to a transition state at an energy relative to the minimum of 828 cm^{-1} and 1523 cm^{-1} in the $\widetilde{\mathrm{X}}$ and $\widetilde{\mathrm{A}}$ electronic states, respectively.

Equilibrium structures were obtained for the $\widetilde{\mathrm{X}}$ and $\widetilde{\mathrm{A}}$ electronic states at the UHF-CCSD(T)/ANO1 level of theory. The optimized geometries show that the $\widetilde{\mathrm{A}} \leftarrow \widetilde{\mathrm{X}}$ [$n \rightarrow \pi^*$] transition induces appreciable changes in the peroxy moiety. The O−O bond elongates ($\Delta r_e = +0.074$), and the C−O bond contracts ($\Delta r_e = -0.017$). These shifts are very similar to those of methyl peroxy radical[26] and ethyl peroxy radicals.[29]

The $\widetilde{\mathrm{A}} \leftarrow \widetilde{\mathrm{X}}$ origin transition (T_0) was computed by extrapolating CCSD(T)/cc-pVXZ energies to the complete basis set limit and adding auxiliary corrections for full triples and perturbative quadruple excitations, core-correlation, relativistic effects, and the Born-Oppenheimer approximation. We predict a T_0 value of 7738 cm^{-1}, which is in excellent agreement with the transitions measured by Sharp, Rupper, and Miller[22] (7755 ± 10 cm^{-1}); Neumark and co-workers (7744 ± 19 cm^{-1}); and Ellison, Lineberger, and co-workers[24] (7799 ± 90 cm^{-1}). Comparison with the values for the methyl peroxy radical (7374 cm^{-1})[26] and ethyl peroxy radical (7363 and 7583 cm^{-1})[29] reflect the trends found in the previous computations of Sharp, Rupper, and Miller.[11]

Anharmonic vibrational frequencies for both electronic states were computed using VPT2+K in conjunction with a hybrid, semi-diagonal quartic force field. Fourteen of the predicted fundamentals (for both the $\widetilde{\mathrm{X}}$ and $\widetilde{\mathrm{A}}$ states) could be directly matched to measured transitions. Among these transitions, there was good agreement between theory and experiment. The most notable discrepancy was the $\widetilde{\mathrm{A}}$-state O−O stretch, which deviated by 25 cm^{-1}. This is ascribed to a combination of basis set incompleteness error and normal mode mismatching, impacting the force constants associated with the O−O stretching and the O−O and C−O stretching degrees of freedom, respectively. The two transitions, at 693 and 760 cm^{-1}, measured in the gas phase infrared study, deviate at least 44 cm^{-1} and 23 cm^{-1} from our fundamentals, respectively, and do not have

obvious assignments.

Conflicts of interest

There are no conflicts to declare.

Acknowledgements

We acknowledge support from the US Department of Energy (DOE), Office of Science, Basic Energy Sciences (BES), Computational and Theoretical Chemistry (CTC) Program and Gas Phase Chemical Physics (GPCP) Program under Contract No. DE-SC0018412.

Appendix: Diagnostics

Table 5: Diagnostics for the reference wavefunction used for the CCSD(T) computations. Diagnostics obtained at the UHF-CCSD(T)/ANO1 equilibrium structures. The C coefficients come from the CASSCF(11,12)/ANO1 wavefunctions.

	$\langle \hat{S}^2 \rangle_{\mathrm{UHF}}$	C_0^2	C_1^2	C_2^2
$\widetilde{\mathrm{X}}\ ^2A''$	0.76	0.95	0.00	0.00
$\widetilde{\mathrm{A}}\ ^2A'$	0.77	0.93	0.02	0.01

Table 6: Non-negligible $\delta\omega$ values denoting the errors from using a UHF reference. Similar values were computed in previous research.[26,31,32,71]

$\widetilde{\mathrm{X}}\ ^2A''$		$\widetilde{\mathrm{A}}\ ^2A'$	
Mode	$\delta\omega$	Mode	$\delta\omega$
ν_{13}	-4	ν_{14}	-18
		ν_{15}	-2
		ν_{16}	-8
		ν_{17}	-1
		ν_{18}	-1

Table 7: Martin diagnostics for identifying significant Fermi resonances. A cut-off of 1 cm^{-1} was used.

$\widetilde{\mathrm{X}}\ ^2A''$		
Modes		Diagnostic
ν_{22}	$2\nu_{39}$	160.8
ν_4	$2\nu_6$	81.1
ν_{10}	$\nu_{16}+\nu_{18}$	26.7
ν_{27}	$\nu_{11}+\nu_{38}$	11.1
ν_{28}	$\nu_{18}+\nu_{34}$	4.2
ν_5	$\nu_6+\nu_8$	4.0
ν_8	$\nu_{15}+\nu_{18}$	3.7
ν_{21}	$2\nu_{39}$	2.9
ν_{26}	$\nu_6+\nu_{28}$	2.8
ν_{26}	$\nu_{22}+\nu_{38}$	1.1
ν_{26}	$\nu_6+\nu_{27}$	1.0
ν_7	$\nu_{15}+\nu_{18}$	1.0

$\widetilde{\mathrm{A}}\ ^2A'$		
Modes		Diagnostic
ν_4	$2\nu_6$	20.3
ν_5	$\nu_6+\nu_8$	3.1
ν_{26}	$\nu_6+\nu_{28}$	2.5
ν_5	$\nu_{37}+\nu_{38}$	1.9
ν_5	$\nu_{37}+\nu_{38}$	1.9
ν_{37}	$\nu_5+\nu_{38}$	1.2
ν_{11}	$\nu_{13}+\nu_{22}$	1.1
ν_{11}	$\nu_{13}+\nu_{22}$	1.1
ν_{38}	$\nu_5+\nu_{37}$	1.1

References

[1] M. J. Pilling and I. W. M. Smith, in *Modern Gas Kinetics: Theory, Experiment, and Application*, Blackwell Scientific Publications, Oxford, United Kingdom, 1987.

[2] S. H. Robertson, P. W. Seakins and M. J. Pilling, in *Low-Temperature Combustion and Autoignition*, Elsevier, San Diego, CA, 1997.

[3] T. Wallington, O. Nielsen and J. Sehested, in *Reactions of Organic Peroxy Radicals in the Gas Phase*, ed. Z. Alfassi, Wiley, 1997, pp. 113–172.

[4] P. Rupper, E. N. Sharp, G. Tarczay and T. A. Miller, *J. Phys. Chem. A*, 2007, **111**, 832–840.

[5] T. J. Wallington, P. Dagaut and M. J. Kurylo, *Chem. Rev.*, 1992, **92**, 667–710.

[6] P. D. Lightfoot, R. A. Cox, J. N. Crowley, M. Destriau, G. D. Hayman, M. E. Jenkin, G. K. Moortgat and F. Zabel, *Atmos. Environ.*, 1992, **26**, 1805–1961.

[7] G. S. Tyndall, R. A. Cox, C. Granier, R. Lesclaux, G. K. Moortgat, M. J. Pilling, A. R. Ravishankara and T. J. Wallington, *J. Geophys. Res.*, 2001, **106**, 12157–12182.

[8] D. Marić, J. N. Crowley and J. P. Burrows, *J. Phys. Chem. A*, 1997, **101**, 2561–2567.

[9] J. A. Jafri and D. H. Phillips, *J. Am. Chem. Soc.*, 1990, **112**, 2586–2590.

[10] O. J. Nielsen and T. J. Wallington, *Ultraviolet Absorption Spectra of Peroxy Radicals in the Gas Phase*, John Wiley & Sons, Chichester, UK, 1997, pp. 69–80.

[11] E. N. Sharp, P. Rupper and T. A. Miller, *Phys. Chem. Chem. Phys.*, 2008, **10**, 3955–3981.

[12] D. A. Parkes and R. J. Donovan, *Chem. Phys. Lett.*, 1975, **36**, 211–214.

[13] D. A. Parkes and R. J. Donovan, *Chem. Phys. Lett.*, 1976, **37**, 198.

[14] G. Chettur and A. Snelson, *J. Phys. Chem.*, 1987, **91**, 5873.

[15] H. E. Hunziker and H. R. Wendt, *J. Chem. Phys.*, 1976, **64**, 3488–3490.

[16] C.-Y. Chung, C.-W. Cheng, Y.-P. Lee, H.-Y. Liao, E. N. Sharp, P. Rupper and T. A. Miller, *J. Chem. Phys.*, 2007, **127**, 044311.

[17] S. Wu, P. Dupré, P. Rupper and T. A. Miller, *J. Chem. Phys.*, 2007, **127**, 224305.

[18] D. B. Atkinson and J. L. Spillman, *J. Phys. Chem. A*, 2002, **106**, 8891–8902.

[19] M. B. Pushkarsky, S. J. Zalyubovsky and T. A. Miller, *J. Chem. Phys.*, 2000, **112**, 10695–10698.

[20] B. G. Glover and T. A. Miller, *J. Phys. Chem. A*, 2005, **109**, 11191–11197.

[21] C. Y. Li, J. Agarwal, C. H. Wu, W. D. Allen and H. F. Schaefer, *J. Phys. Chem. B*, 2015, **119**, 728–735.

[22] E. N. Sharp, P. Rupper and T. A. Miller, *J. Phys. Chem. A*, 2008, **112**, 1445–1456.

[23] S. J. Blanksby, T. M. Ramond, G. E. Davico, M. R. Nimlos, S. Kato, V. M. Bierbaum, W. C. Lineberger, G. B. Ellison and M. Okumura, *J. Am. Chem. Soc.*, 2001, **123**, 9585–9596.

[24] E. P. Clifford, P. G. Wenthold, R. Gareyev, W. C. Lineberger, C. H. DePuy, V. M. Bierbaum and G. B. Ellison, *J. Chem. Phys.*, 1998, **109**, 10293–10310.

[25] J. A. DeVine, M. L. Weichman, M. C. Babin and D. M. Neumark, *J. Chem. Phys.*, 2017, **147**, 013915.

[26] A. V. Copan, H. F. Schaefer and J. Agarwal, *Mol. Phys.*, 2015, **113**, 2992–2998.

[27] J. Agarwal, A. C. Simmonett and H. F. Schaefer, *Mol. Phys.*, 2012, **110**, 2419–2427.

[28] A. M. Morrison, J. Agarwal, H. F. Schaefer and G. E. Douberly, *J. Phys. Chem. A*, 2012, **116**, 5299–5304.

[29] A. M. Launder, J. M. Turney, J. Agarwal and H. F. Schaefer, *Phys. Chem. Chem. Phys.*, 2017, **19**, 15715–15723.

[30] P. R. Hoobler, J. M. Turney and H. F. Schaefer, *J. Chem. Phys.*, 2016, **145**, 174301.

[31] A. V. Copan, A. E. Wiens, E. M. Nowara, H. F. Schaefer and J. Agarwal, *J. Chem. Phys.*, 2015, **142**, 054303.

[32] S. N. Elliott, J. M. Turney and H. F. Schaefer, *RSC Adv.*, 2015, **5**, 107254–107265.

[33] K. B. Moore, J. M. Turney and H. F. Schaefer, *J. Chem. Phys.*, 2017, **146**, 194304.

[34] P. J. Knowles, C. Hampel and H.-J. Werner, *J. Chem. Phys.*, 2000, **112**, 3106.

[35] P. J. Knowles, C. Hampel and H.-J. Werner, *J. Phys. Chem.*, 1993, **99**, 5219–5227.

[36] J. D. Watts, J. Gauss and R. J. Bartlett, *J. Chem. Phys.*, 1993, **98**, 8718–8733.

[37] *CFOUR, A Quantum Chemical Program Package Written by J.F. Stanton, J. Gauss, M.E. Harding, P.G. Szalay with contributions from A.A. Auer, R.J. Bartlett, U. Benedikt, C. Berger, D.E. Bernholdt, Y.J. Bomble, L. Cheng, O. Christiansen, M. Heckert, O. Heun, C. Huber, T.-C. Jagau, D. Jonsson, J. Jusélius, K. Klein, W.J. Lauderdale, D.A. Matthews, T. Metzroth, L.A. Mück, D.P. O'Neill, D.R. Price, E. Prochnow, C. Puzzarini, K. Ruud, F. Schiffmann, W. Schwalbach, C. Simmons, S. Stopkowicz, A. Tajti, J. Vázquez, F. Wang, J.D. Watts and the integral packages MOLECULE (J. Almlöf and P.R. Taylor), PROPS (P.R. Taylor), ABACUS (T. Helgaker, H.J. Aa. Jensen, P. Jørgensen, and J. Olsen), and ECP Routines by A. V. Mitin and C. van Wüllen. For the Current Version, see http://www.cfour.de.*

[38] J. Almlöf and P. R. Taylor, *J. Chem. Phys.*, 1987, **86**, 4070–4077.

[39] L. McCaslin and J. Stanton, *Mol. Phys.*, 2013, **111**, 1492–1496.

[40] M. S. Schuurman, S. R. Muir, W. D. Allen and H. F. Schaefer, *J. Chem. Phys.*, 2004, **120**, 11586–11599.

[41] J. M. Gonzales, C. Pak, R. S. Cox, W. D. Allen, H. F. Schaefer, A. G. Császár and G. Tarczay, *Chem. Eur. J.*, 2003, **9**, 2173–2192.

[42] A. G. Császár, W. D. Allen and H. F. Schaefer, *J. Chem. Phys.*, 1998, **108**, 9751–9764.

[43] A. L. L. East and W. D. Allen, *J. Chem. Phys.*, 1993, **99**, 4638–4650.

[44] T. H. Dunning, *J. Chem Phys.*, 1989, **90**, 1007–1023.

[45] A. Karton and J. M. L. Martin, *Theor. Chem. Acc.*, 2006, **115**, 330–333.

[46] T. Helgaker, W. Klopper, H. Koch and J. Noga, *J. Chem. Phys.*, 1997, **106**, 9639–9646.

[47] D. Feller, *J. Chem. Phys.*, 1992, **96**, 6104–6114.

[48] K. A. Peterson, D. E. Woon and T. H. Dunning, *J. Chem Phys.*, 1994, **100**, 7410–7415.

[49] D. W. Schwenke, *J. Chem Phys.*, 2005, **122**, 014107.

[50] J. M. L. Martin, *Chem. Phys. Lett.*, 1996, **259**, 669–678.

[51] W. J. Hehre, R. Ditchfield and J. A. Pople, *J. Chem. Phys.*, 1972, **56**, 2257–2261.

[52] Harihara.Pc and J. A. Pople, *Theoretica Chimica Acta*, 1973, **28**, 213–222.

[53] D. E. Woon and T. H. Dunning, *J. Chem. Phys.*, 1995, **103**, 4572–4585.

[54] N. C. Handy, Y. Yamaguchi and H. F. Schaefer, *J. Chem. Phys.*, 1986, **84**, 4481–4484.

[55] H. Sellers and P. Pulay, *Chem. Phys. Lett.*, 1984, **103**, 463–465.

[56] G. Tarczay, A. G. Császár, W. Klopper and H. M. Quiney, *Mol. Phys.*, 2001, **99**, 1769–1794.

[57] W. Klopper, *J. Comput. Chem.*, 1997, **18**, 20–27.

[58] M. S. Schuurman, W. D. Allen, P. V. Schleyer and H. F. Schaefer, *J. Chem. Phys.*, 2005, **122**, 104302.

[59] Mrcc, *A Quantum Chemical Program Suite Written by M. Kállay, Z. Rolik, I. Ladjánszki, L. Szegedy, B. Ladóczki, J. Csontos, and B. Kornis.*

[60] Z. Rolik, L. Szegedy, I. Ladjánszki, B. Ladóczki and M. Kállay, *J. Chem. Phys.*, 2013, **139**, 094105.

[61] D. A. Clabo, W. D. Allen, R. B. Remington, Y. Yamaguchi and H. F. Schaefer, *Chem. Phys.*, 1988, **123**, 187–239.

[62] J. D. Watts, J. Gauss and R. J. Bartlett, *Chem. Phys. Lett.*, 1992, **200**, 1–7.

[63] J. Breidung, W. Thiel, J. Gauss and J. F. Stanton, *J. Chem. Phys.*, 1999, **110**, 3687–3696.

[64] A. M. Rosnik and W. F. Polik, *Mol. Phys.*, 2014, **112**, 261–300.

[65] D. A. Clabo, W. D. Allen, R. B. Remington, Y. Yamaguchi and H. F. Schaefer, *Chem. Phys.*, 1988, **123**, 187–239.

[66] D. A. Matthews, J. Vazquez and J. F. Stanton, *Mol. Phys.*, 2007, **105**, 2659–2666.

[67] J. M. L. Martin, T. J. Lee, P. R. Taylor and J. François, *J. Chem. Phys.*, 1995, **103**, 2589–2602.

[68] P. R. Franke, D. P. Tabor, C. P. Moradi, G. E. Douberly, J. Agarwal, H. F. Schaefer and E. L. Sibert, *J. Chem. Phys.*, 2016, **145**, 224304.

[69] P. L. Raston, J. Agarwal, J. M. Turney, H. F. Schaefer and G. E. Douberly, *J. Chem. Phys.*, 2013, **138**, 194303.

[70] V. Barone, *J. Chem. Phys.*, 2005, **122**, 014108.

[71] M. L. Estep and H. F. Schaefer, *Phys. Chem. Chem. Phys.*, 2016, **18**, 22293–22299.

[72] H.-J. Werner and P. J. Knowles, *J. Chem. Phys.*, 1985, **82**, 5053–5063.

[73] T. Busch, A. D. Esposti and H.-J. Werner, *J. Chem. Phys.*, 1991, **94**, 6708–6715.

[74] G. M. P. Just, A. B. McCoy and T. A. Miller, *J. Chem. Phys.*, 2007, **127**, 044310.

[75] P. S. Thomas and T. A. Miller, *Chem. Phys. Lett.*, 2010, **491**, 123–131.

[76] P. S. Thomas and T. A. Miller, *Chem. Phys. Lett.*, 2011, **514**, 196–201.

[77] T. D. Crawford, J. F. Stanton, W. D. Allen and H. F. Schaefer, *J. Chem. Phys.*, 1997, **107**, 10626.

[78] P. R. Franke, J. T. Brice, C. P. Moradi, H. F. Schaefer and G. E. Douberly, *J. Phys. Chem. A*, 2019, **123**, accepted.

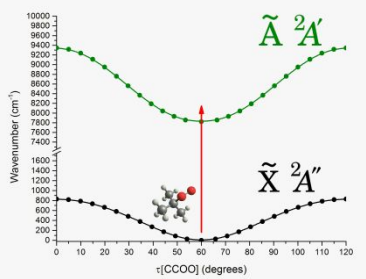

The lowest adiabatic electronic transition origin and fundamental vibrational frequencies are computed, with high accuracy, for *tert*-butyl peroxy radical.